Open Archive Toulouse Archive Ouverte (OATAO)

OATAO is an open access repository that collects the work of Toulouse researchers and makes it freely available over the web where possible.

Any correspondence concerning this service should be sent to the repository administrator: staff-oatao@inp-toulouse.fr

Local electrochemical impedance spectroscopy: Considerations about the cell geometry

Isabelle Frateur [a,1], Vicky Mei-Wen Huang [b], Mark E. Orazem [b,1],
Nadine Pébère [c,1], Bernard Tribollet [d,1], Vincent Vivier [d,*,1]

[a] *LPCS, CNRS – ENSCP (UMR 7045), Ecole Nationale Supérieure de Chimie de Paris,
11 rue Pierre et Marie Curie, 75005 Paris, France*
[b] *Department of Chemical Engineering, University of Florida, Gainesville, FL 32611, USA*
[c] *CIRIMAT, UMR 5085 du CNRS, ENSIACET, 118 route de Narbonne, 31077 Toulouse Cedex 04, France*
[d] *LISE, UPR 15 du CNRS, Université P. et M. Curie, CP 133, 4 Place Jussieu, 75252 Paris Cedex 05, France*

Abstract

Local electrochemical impedance spectroscopy provides a powerful tool for the investigation of surface heterogeneities on electrode surfaces. However, measurements are greatly influenced by geometry-induced frequency dispersion. In order to account for this frequency dispersion, both simulations and experiments were performed to explore the influence of a recessed electrode on the local and global impedance response. The calculations presented here demonstrated that the depth of the recessed electrode required to achieve a uniform primary current distribution was twice the electrode radius. The calculations provide guidelines for design of LEIS measurements, and were in good agreement with results obtained for a stainless steel disk electrode in a Na_2SO_4 electrolyte.

1. Introduction

In conventional electrochemical experiments such as electrochemical impedance spectroscopy (EIS) [1,2], the electrode response to a perturbation signal corresponds to a surface-averaged measurement ascribable to the behavior of the whole electrode surface. However, electrochemical systems rarely show an ideal behavior leading to difficulties with data interpretation. For instance, the use of the usual planar disk electrodes embedded in an insulator induces current and potential distributions as previously shown by Newman et al. [3–5]. They demonstrated that the potential distribution is not uniform under conditions where the current density is uniform, and conversely the current distribution is not uniform under conditions where the primary potential is uniform. Moreover, in the case of heterogeneous surface reactivity such as in localized corrosion (passive metals), surface-averaged techniques cannot identify the location of the attack, the initiation zone nor the local mechanisms responsible of the breakdown of the passive film [6].

To overcome these difficulties, several scanning techniques using small electrodes such as metal microelectrodes have been developed to probe *in situ* the electrochemical interface. Among them, the local electrochemical impedance spectroscopy (LEIS) performed on restricted active areas was pioneered by Isaacs et al. [7–9]. A significant contribution was the development of a novel method for generating quantitative LEIS [8,9], which was based on the assumption that the local impedance can be generated by measuring the ac–local-current density in the vicinity of the working electrode in a usual three-electrode cell configuration. From a practical point of view, this was achieved with the use of a dual microelectrode for sensing the local ac–potential gradient, the local current being obtained from the direct application of the Ohm's law [8–10]. Using this kind of experimental set-up, impedance diagrams over an active pit were obtained allowing the direct comparison of local and global impedances [11]. Some LEIS investigations were also reported using larger

* Corresponding author.
E-mail address: vincent.vivier@courriel.upmc.fr (V. Vivier).
[1] ISE member.

probes. For instance, Baril et al. [12] investigated the electrochemical behavior of the AZ91 magnesium alloy in Na_2SO_4 solution, whereas Philippe et al. [13] investigated polymer-coated galvanized steel.

In a recent series of papers [14–17], our group has undertaken an analysis of the basis of the LEIS technique when it is applied to a disk electrode. A key contribution was the definition of three local impedances. The local interfacial impedance (z_0) was defined to involve both a local current density and the local potential drop across the diffuse double layer. The local Ohmic impedance (z_e) was defined to involve a local current density and potential drop from the outer region of the diffuse double layer to the distant reference electrode. The local impedance (z) was thus the sum of the local interfacial impedance and the local Ohmic impedance. Moreover, the influence of probe height over a disk electrode was explored theoretically in a previous work [17]. The calculated and experimentally observed frequency dispersion and imaginary contributions to Ohmic impedance were attributed to the current and potential distributions associated with the typical geometry of a disk electrode embedded in an insulating plane. This previous work suggests that the frequency dispersion effects should not be apparent for geometries, such as recessed or spherical electrodes, for which the primary current distribution is uniform.

The objective of the present work is to explore the influence of the recessed geometry of a disk electrode on the local and global impedance responses. Both theoretical basis and experimental results will be presented to demonstrate the power of LEIS for the study of surface reactivity.

2. Experimental

2.1. Probe preparation and cell design

The disk electrode used in the experimental part was a commercial 316 L stainless steel, 1 mm thick and with a diameter of 5 cm. The electrochemical measurements were carried out with a classical three-electrode cell at room temperature as sketched in Fig. 1. The cell consisted of two independent cylinders made of Bakelite® which were fit together by compression. The upper part of the cell was 10 cm in diameter and 5 cm height. The lower cylinder was 5 cm in diameter and its height, p, could be 1, 5 or 10 cm. The steel disk was fixed at the bottom of the cylinder with an O-ring. The counterelectrode was a large platinum grid surrounding all the cell and the potentials were measured with respect to a saturated sulfate electrode (SSE) located far from the sample in the bulk solution. The dual-probe (or bi-electrode) consisted of two Pt microwires (Goodfellow), both of 40 μm in diameter. Wires were sealed into a bi-capillary by melting the glass using a resistance heater with a controllable current through a coiled nichrome wire. The tip was then polished with SiC paper down to grade 1200 and a deposit of Pt black from hydrogen hexachloroplatinate(IV) was performed daily on each microdisk to reduce the interfacial impedance of these electrodes [18]. The electrolyte was a 0.1 M Na_2SO_4 solution prepared
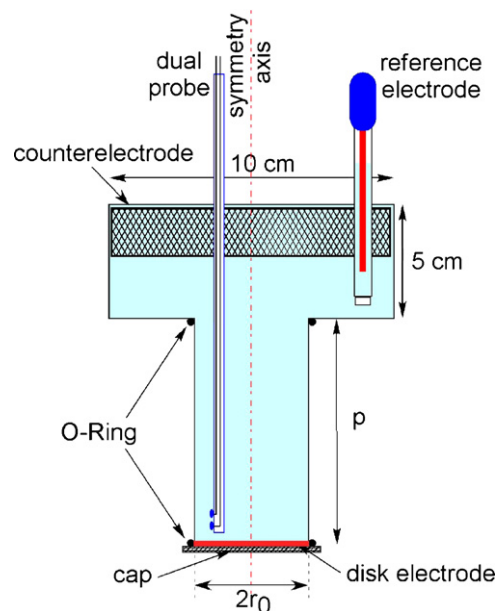

Fig. 1. Schematic representation of the electrochemical cell used as recessed system.

from analytical grade chemical (Aldrich) used in deionized water.

2.2. Electrochemical device

The experimental set-up consisted of a home-made potentiostat coupled with a four-channel frequency response analyzer (FRA, Solartron 1254), allowing both global and local impedances to be recorded simultaneously. Two home-made analog differential amplifiers with both variable gain and high input impedance were used to record simultaneously the local potential and current variations. The bi-electrode was moved with a 3-axis positioning system (UTM25, Newport) driven by a motion encoder (MM4005, Newport) allowing a spatial resolution of 0.2 μm in the three directions. All measurements were performed under potentiostatic regulation, with 50 acquisition cycles, seven points per decade of frequency, and a 50 mV peak-to-peak amplitude applied sinusoidal voltage. This last value was chosen to be as large as possible to improve the signal/noise ratio but sufficiently low so that the linear approximation of the potential/current curve can be used. Home-made software developed for scanning electrochemical microscopy was used for data acquisition [19,20].

3. Definitions and mathematical development

Using a bi-electrode for probing the solution potential and a four-channel frequency response analyzer, global, local, and local interfacial impedances could be measured simultaneously [14]. In the following, the use of an upper-case letter signifies that Z is a global value; whereas, the use of a lower-case letter means that z is a local value, following the notation proposed by Huang et al. [14] and summarized in Appendix A. For local electrochemical measurements, the local ac–current density $i_{loc}(\omega)$

was obtained through the Ohm's law using

$$i_{\text{loc}}(\omega) = \frac{\Delta V_{\text{probe}}(\omega)\kappa}{d} \qquad (1)$$

where κ is the electrolyte conductivity, $\Delta V_{\text{probe}}(\omega)$ is the ac–potential difference between the two probes, and d is the distance between the two probes.

The local impedance (z) involves the electrode potential measured with respect to a reference electrode located far from the electrode surface

$$z(\omega) = \frac{\tilde{V}(\omega) - \Phi_{\text{ref}}}{i_{\text{loc}}(\omega)} = \frac{\tilde{V}(\omega)}{\Delta V_{\text{probe}}(\omega)} \frac{d}{\kappa} \qquad (2)$$

where $\tilde{V}(\omega) - \Phi_{\text{ref}}$ represents the ac–potential difference between the electrode surface and the reference electrode in the bulk solution.

The local interfacial impedance (z_0) involves the potential of the electrode referenced to the potential of the electrolyte (Φ_0) measured at the inner limit of the diffusion layer

$$z_0(\omega) = \frac{\tilde{V}(\omega) - \check{\Phi}_0(\omega)}{i_{\text{loc}}(\omega)} = \frac{\tilde{V}(\omega) - \check{\Phi}_0(\omega)}{\Delta V_{\text{probe}}(\omega)} \frac{d}{\kappa} \qquad (3)$$

Thus the local Ohmic impedance (z_e) can be deduced by calculating the difference between the local impedance and local interfacial impedance

$$z_e(\omega) = z(\omega) - z_0(\omega) \qquad (4)$$

From a practical point of view, it is not possible to perform a potential measurement just outside the double layer (Fig. 2). Thus, the distance between the probe and the disk electrode, h, must be taken into account. Using the definitions presented above, the local interfacial impedance, $z_h(\omega)$, estimated at $y = h$,
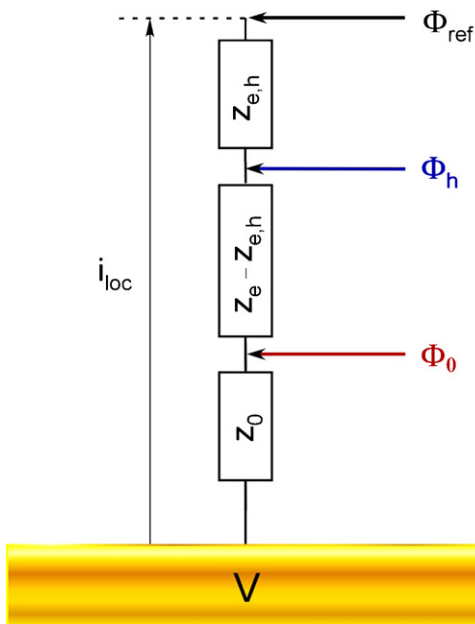

Fig. 2. Electrical equivalent representation of the local impedance.

was obtained using

$$z_h(\omega) = \frac{\tilde{V}(\omega) - \tilde{\Phi}_h}{i_{\text{loc}}(\omega)} = \frac{\tilde{V}(\omega) - \tilde{\Phi}_h}{\Delta V_{\text{probe}}(\omega)} \frac{d}{\kappa} \qquad (5)$$

where $\tilde{V}(\omega) - \tilde{\Phi}_h$ represents the ac–potential difference between the electrode surface and the closest of the two probes of the bi-electrode, located at a distance $y = h$ from the electrode surface (Fig. 2). The local Ohmic impedance $z_{e,h}$ can thus be deduced by calculating the difference between the local impedance and local interfacial impedance, i.e.

$$z_{e,h}(\omega) = z(\omega) - z_h(\omega) \qquad (6)$$

The mathematical development follows that presented by Newman for a planar disk electrode embedded in a coplanar insulator [21], and this model was extended to a recessed geometry (Fig. 1) in order to investigate the edge effect of the electrode on the electrochemical impedance response. The geometry of the system was defined by the radius of the electrode r_0, and by the depth of the recessed electrode p. The potential Φ in solution surrounding this electrode is governed by Laplace's equation

$$\nabla^2 \Phi = 0 \qquad (7)$$

Using cylindrical coordinates (r,θ,y), it can be expressed as

$$\frac{1}{r} \frac{\partial}{\partial r} \left(r \frac{\partial \Phi}{\partial r} \right) + \frac{1}{r^2} \frac{\partial^2 \Phi}{\partial \theta^2} + \frac{\partial^2 \Phi}{\partial y^2} = 0 \qquad (8)$$

where y is the normal distance to the electrode surface, r is the radial coordinate, and θ is the azimuth. The cylindrical symmetry condition requires that the geometry is invariant under rotation about the y axis, thus

$$\frac{\partial \Phi}{\partial \theta} = 0 \qquad (9)$$

On the surrounding insulator and far from the electrode surface, the boundary conditions were given by

$$\left. \frac{\partial \Phi}{\partial y} \right|_{y=0} = 0 \quad \text{at } r > r_0 \qquad (10)$$

and

$$\Phi \to 0 \quad \text{as } r^2 + y^2 \to \infty \qquad (11)$$

For a capacitive behavior, the flux boundary condition at the electrode surface was written as

$$j\omega C_0(\tilde{V} - \tilde{\Phi}_0) = -\kappa \left. \frac{\partial \tilde{\Phi}}{\partial y} \right|_{y=0} \qquad (12)$$

where C_0 is the interfacial capacitance, κ is the electrolyte conductivity, V is the electrode potential, and Φ_0 is the potential just outside the double layer. In the case of a CPE behavior, the governing equations were similar, the only change to be done was the substitution of the admittance $j\omega C_0$ in Eq. (12) by $Q(j\omega)^\alpha$. The current density was thus calculated by integrating the local admittance of the system over the disk electrode surface. As previously observed for a planar embedded disk

electrode [14–16], the results could be expressed in terms of a dimensionless frequency, K, which is defined by

$$K = \frac{Q\omega^\alpha r_0}{\kappa} \qquad (13)$$

in which α is taken to unity and $Q = C_0$ in the case of a pure capacitor.

For data analysis, the origin of the normal axis $y = 0$ is always defined by the disk electrode surface, and all reported distances were measured from this origin. All calculations were performed using finite element package FEMLAB with the conductive media DC module in a 2D axial symmetry. The geometry and the position of the reference electrode were shown to play a significant role on the numerical result of the calculated impedance. Thus, a spherical geometry and a distance 2000 times larger than the disk electrode radius were used to perform numerical calculation in order to reach an error range smaller than 0.2%.

4. Results

4.1. Electrode with a pure capacitive behavior

The calculated global impedance response of the electrode is presented in Fig. 3 with the dimensionless depth P ($P = p/r_0$) as a parameter. These calculations were performed for a pure capacitor (50 µF cm^{-2}) assuming that reference and counterelectrode were at infinity. The impedance was made dimensionless according to $Z\kappa/r_0\pi$ in which the units of the impedance Z are assumed to be scaled by the electrode area, and the dimensionless frequency $K = \omega C_0 r_0/\kappa$ accounts for the dimension and capacity of the electrode. Thus, the Nyquist representation of the complex-impedance data presented in Fig. 3 applies for all values of electrolyte conductivity and disk radius. For a slightly recessed electrode ($P = 0.004$), the frequency dispersion observed in the high frequency range is in good agreement with the previous work of Newman [21] for a planar disk electrode ($P = 0$, for which the high-frequency limit for the real impedance is equal to 1/4) and plotted in the same figure. In the low frequency range ($K < 1$) the electrode response exhibits a pure capacitive behavior. When the depth of the recessed electrode is increased, the frequency dispersion decreases; whereas, the Ohmic part of the impedance is increased due to the Ohmic contribution of the electrolyte in the recessed electrode.

The influence of the depth of the recessed electrode is seen more clearly in the Nyquist representation of the corrected
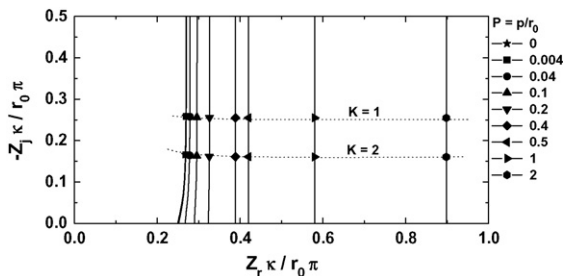

Fig. 3. Nyquist representation of the global impedance of an ideally polarized electrode with the depth of the recessed electrode as a parameter.
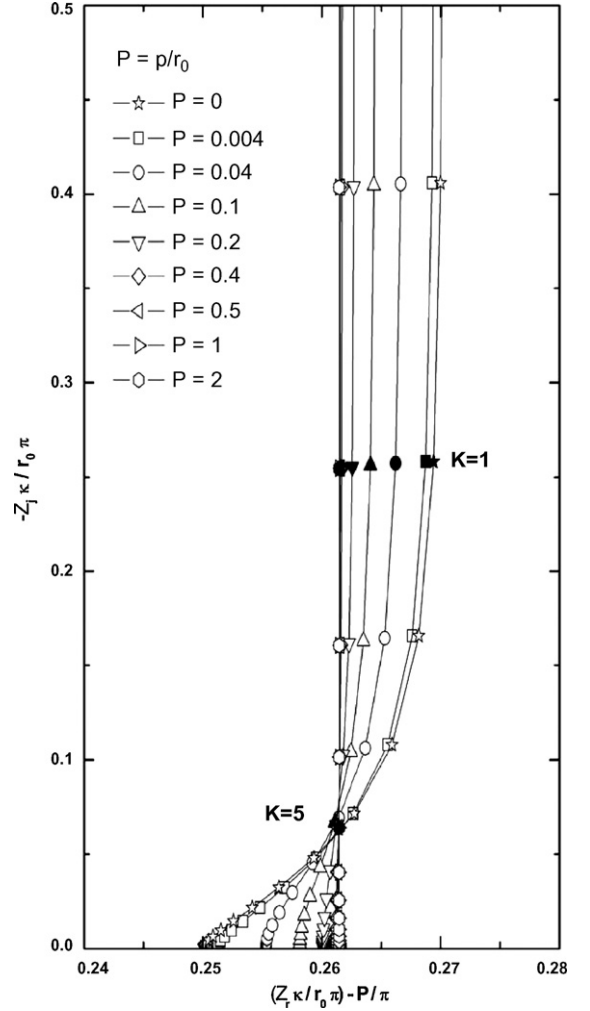

Fig. 4. Nyquist representation of the global impedance of an ideally polarized electrode corrected from the Ohmic contribution with the depth of the recessed electrode as a parameter. Non-isotropic coordinates are used to emphasize the time-constant dispersion seen at higher frequencies. For $P = 0$ and $P = 0.004$, points are superimposed.

impedance shown in Fig. 4. This corrected impedance was obtained from the global impedance by subtracting P/π which corresponds to the dimensionless resistive contribution of the electrolyte in the cylinder of base radius r_0 and height p, and non-isotropic coordinates are used in Fig. 4 to emphasize the time-constant dispersion seen at higher frequencies. When the depth is larger than the diameter of the electrode ($P > 2$) the frequency dispersion can be neglected and the impedance diagrams superposed for the whole frequencies. For slightly recessed electrodes ($P < 2$), the Nyquist representation shows that the high frequency parts of the impedance spectrum are centered on the value 0.261. Moreover, the low frequency limit of this corrected impedance depends on the depth of the recessed electrode and an invariant point is observed for $K = 5$.

The calculated local impedance is presented in Fig. 5 with normalized radial position as a parameter for a small recessed parameter value ($P = 0.004$) at the electrode surface ($H = 0$, H being the dimensionless probe-to-electrode distance, $H = h/r_0$). The dimensionless impedance is scaled to the disk area for an
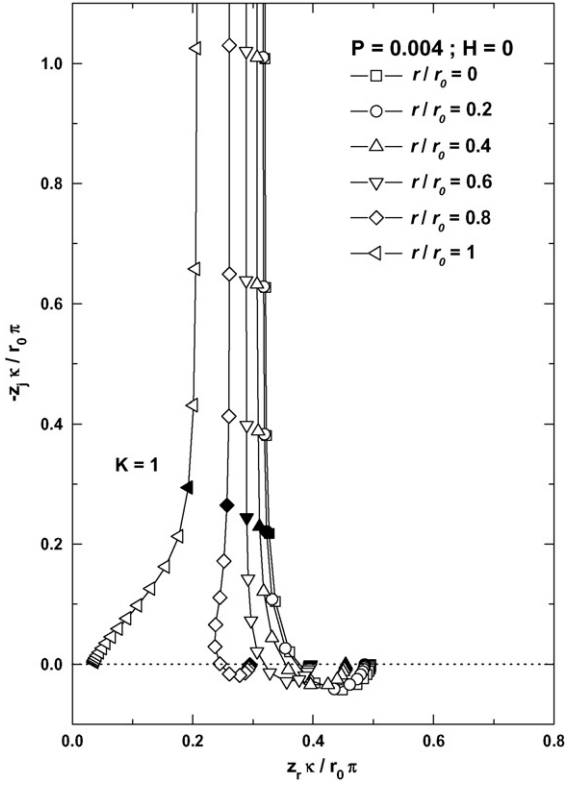
Fig. 5. Nyquist representation of the local impedance of an ideally polarized electrode with the radial position as a parameter for a slightly recessed electrode ($P = 0.004$).

frequencies are characterized by an inductive loop; whereas, at the periphery of the electrode, the high frequencies exhibit a capacitive behavior. Moreover, all these diagrams are centered on the asymptotic value of 0.25 for the high-frequency global Ohmic resistance.

Frateur et al. [17] have shown that the height, h, of the LEIS probe over the electrode surface plays a critical role on the local impedance response. The combined influence of the height of the LEIS probe over the electrode surface and the depth of the recessed electrode is reported in Figs. 6–8 with the radial position of the probe as a parameter. To have a better visualization and to facilitate interpretation of the results, a cartoon was placed in the upper right corner of each figure to provide a representation of the depth of the recessed electrode and the probe-to-disk electrode distance.

At a recessed depth of $P = 0.5$, shown in Fig. 6, the local impedance at the electrode surface ($H = 0$) shows a high-frequency capacitive loop at the periphery of the electrode and a high-frequency inductive loop at the center of the electrode (Fig. 6a). The high-frequency features become less apparent as the sensing electrode is raised ($H = 0.25$ and $H = 0.5$), but the real part of the low-frequency local impedance becomes a strong function of radial position (Fig. 6b and c). This feature arises due to the nonuniform axial current distribution near the mouth of the recessed electrode. The impedance is smallest at large radial positions where the current density is largest and is largest at the center where the current density is smallest. The influence of frequency dispersion is still evident at the electrode surface ($H = 0$) for $P = 1$, shown in Fig. 7; however, the frequency dispersion becomes negligible when the dimensionless probe-to-electrode distance is larger than 0.5 (Fig. 7b and c).

The observations that all local impedance calculations converge at the electrode surface ($H = 0$) for $P = 2$ (Fig. 8) and that the impedance follows a vertical line on a Nyquist plot indicate the absence of frequency dispersion. A recessed electrode for which $P = 2$ is thus sufficient to eliminate frequency dispersive

easiest comparison with global impedance diagrams. The results obtained here for local impedance are very similar to those previously reported for an ideally polarized embedded disk electrode [14]. The impedance is the largest at the center of the electrode and smaller at the periphery reflecting the greater accessibility at the edge of the disk electrode. At the electrode center, the high
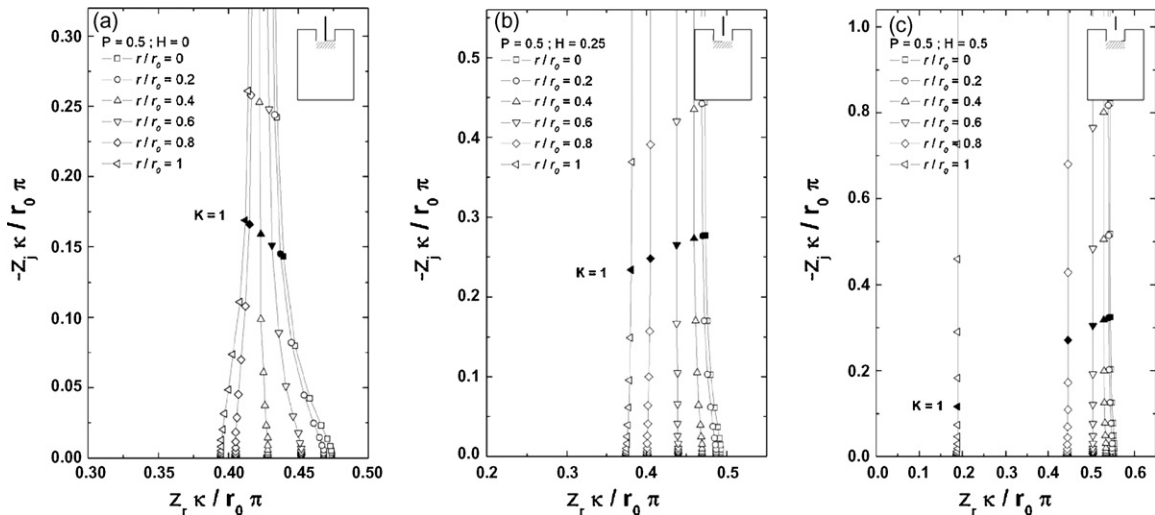

Fig. 6. Nyquist representation of the local impedance of an ideally polarized electrode with the radial position as a parameter for a recessed electrode depth equal to the half radius of the electrode: (a) at the electrode surface; (b) in the middle of the recessed electrode; (c) at the mouth of the recessed electrode.
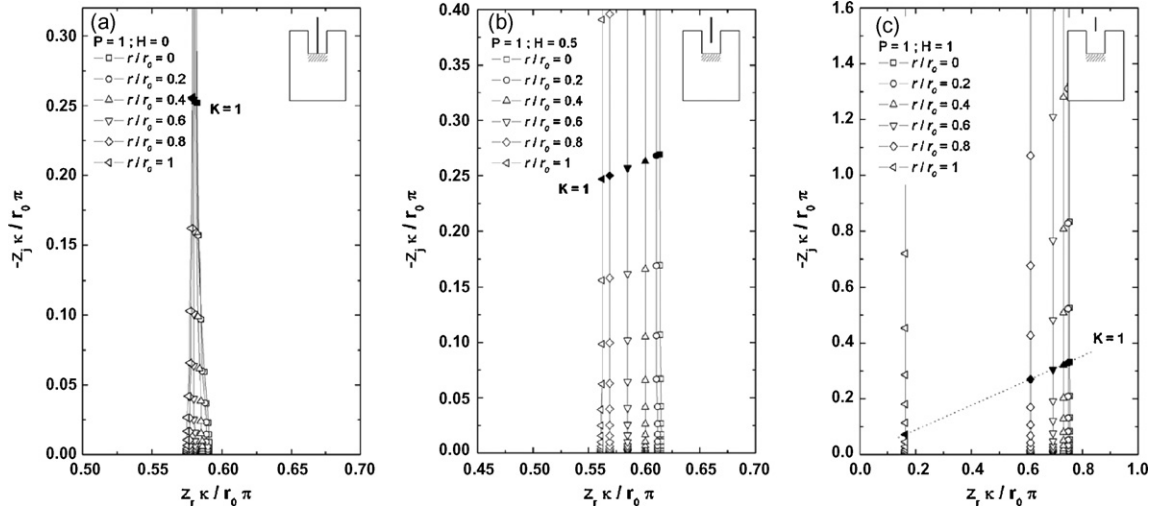
Fig. 7. Nyquist representation of the local impedance of an ideally polarized electrode with the radial position as a parameter for a recessed electrode depth equal to the electrode radius: (a) at the electrode surface; (b) in the middle of the recessed electrode; (c) at the mouth of the recessed electrode.

effects. The influence of the mouth of the recessed electrode is already evident at $H = 1$ in the radial dependence of the real part of the local impedance. The radial distribution is most prominent for $H = 2$.

Huang et al. [14–16] have shown that, for a disk electrode in an insulating plane, the Ohmic impedance is a complex number with non-negligible imaginary components in the frequency range near $K = 1$. The Ohmic impedance for a recessed electrode is presented in Fig. 9 for a radial position at the center of the electrode. At the mouth of the recessed electrode, Fig. 9a, the local Ohmic impedance has an inductive loop for small values of P, but approaches a frequency-independent fixed value for larger values of P. The local Ohmic impedance at the electrode surface is presented in Fig. 9b in which the real part is corrected from the Ohmic contribution of the recess. On this scale, it is obvious that a complex inductive character is seen for the local Ohmic impedance for $P \leq 1$ and that the local Ohmic impedance approaches a frequency-independent

fixed value for $P = 2$. The corresponding results for $r/r_0 = 0.6$ are presented in Fig. 10. The local Ohmic impedance has a capacitive character at the mouth of the recessed electrode (Fig. 10a) and an inductive character at the electrode surface (Fig. 10b).

4.2. Blocking electrode with CPE behavior

The calculated dimensionless impedance response of a recessed electrode ($P = 0.1$) with a local CPE behavior ($Q = 100 \times 10^{-6}\ \Omega^{-1}\ \text{cm}^{-2}\ \text{s}^{\alpha}$) is presented in Fig. 11 in Nyquist representation with α as a parameter. In the high frequencies, the real part of the impedance tends towards the expected value of 0.29, which corresponds to the theoretical contribution of an embedded planar disk electrode [21] plus the Ohmic contribution of the recessed electrode. In the low frequency range, the slope of the impedance spectra depends on the value of α.
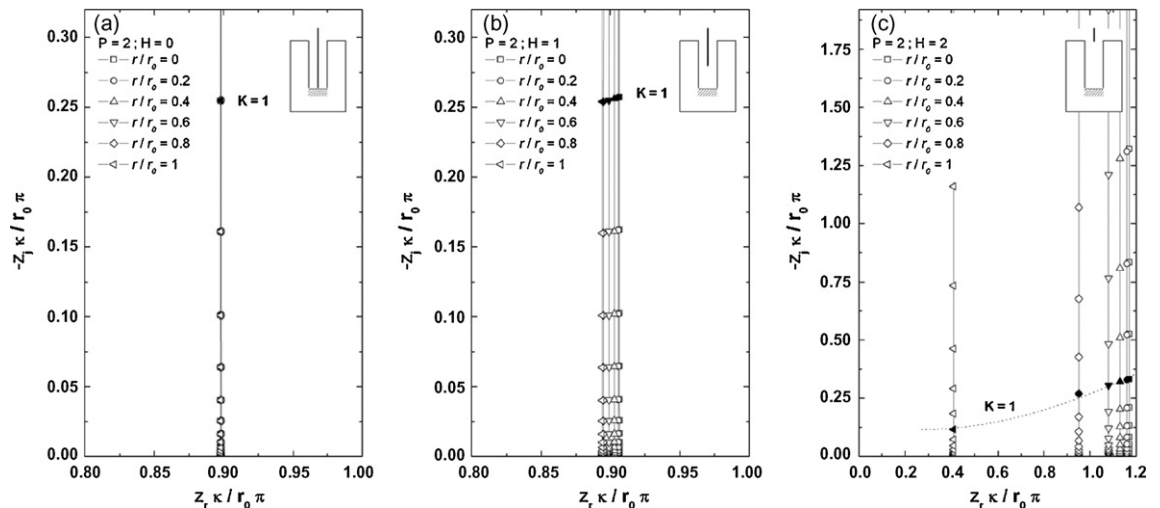

Fig. 8. Nyquist representation of the local impedance of an ideally polarized electrode with the radial position as a parameter for a recessed electrode depth equal to the electrode diameter: (a) at the electrode surface; (b) in the middle of the recessed electrode; (c) at the mouth of the recessed electrode.
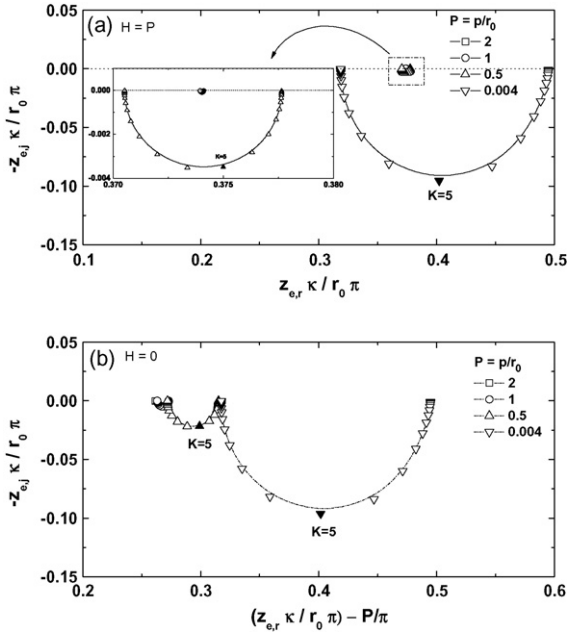
Fig. 9. Local Ohmic impedance at $r/r_0 = 0$ at the mouth of the recessed electrode (a) and at the electrode surface (b) with the recessed electrode depth as a parameter.

The calculated local impedance in Nyquist format at the center of a recessed electrode ($P = 0.1$) for a local CPE ($\alpha = 0.8$, $Q = 100 \times 10^{-6}\ \Omega^{-1}\ \mathrm{cm}^{-2}\ \mathrm{s}^{0.8}$) is presented in Fig. 12 with the normalized probe-to-electrode distance as a parameter. The impedance in the high frequency domain is characterized by an inductive loop, and its magnitude depends on the verti-
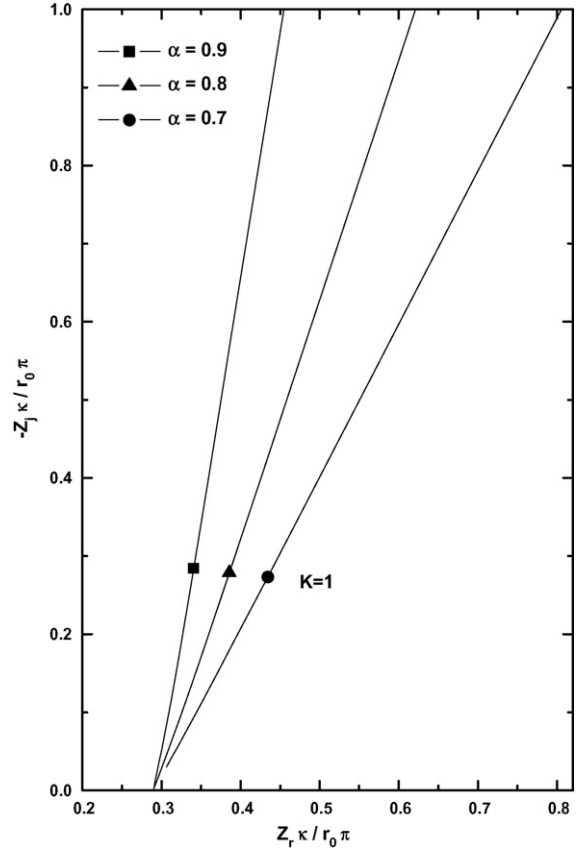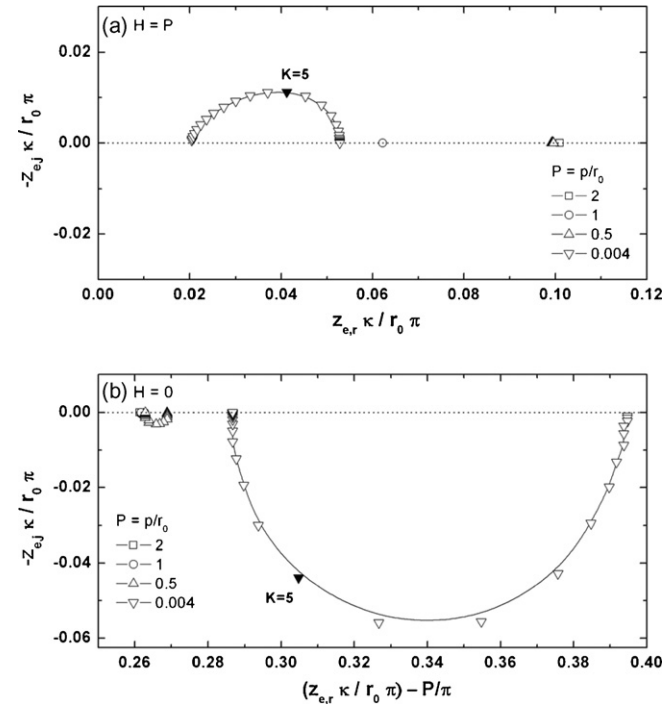

Fig. 11. Nyquist representation of the global impedance of a recessed electrode ($P = 0.1$) with a local CPE ($Q = 100 \times 10^{-6}\ \Omega^{-1}\ \mathrm{cm}^{-2}\ \mathrm{s}^{\alpha}$) with α as a parameter.

cal location of the probe. In the low frequency range, the magnitude of the impedance response also depends on the distance H, and the local impedance always exhibits a CPE behavior with a constant value of 0.8 at low frequencies. Moreover, a frequency shift is observed depending on the probe location.

Fig. 13 shows the local Ohmic impedance in Nyquist format for a recessed electrode ($P = 0.1$) for a local CPE ($\alpha = 0.8$, $Q = 100 \times 10^{-6}\ \Omega^{-1}\ \mathrm{cm}^{-2}\ \mathrm{s}^{0.8}$) at the mouth of the recessed electrode (a); in the middle of the recessed electrode (b); at the electrode surface (c) with the normalized radial position of the probe as a parameter. The results obtained here are very similar to those reported for an ideally polarized electrode and for a blocking disk electrode with a local CPE behavior [14,15]. At the periphery of the electrode, two-time constants (inductive and capacitive loops) are seen, but the inductive behavior diminishes as the probe is withdrawn from the disk-electrode surface. At the electrode center, only an inductive loop is shown with amplitude that slightly increases when the probe-to-electrode distance diminishes. Moreover, no significant frequency shift can be seen when varying the probe height. As expected, the local impedance diagrams for local CPE behavior only differs from those with a pure capacitance behavior by both a frequency shift of the time constant and a low frequency behavior that depends on the value of α.
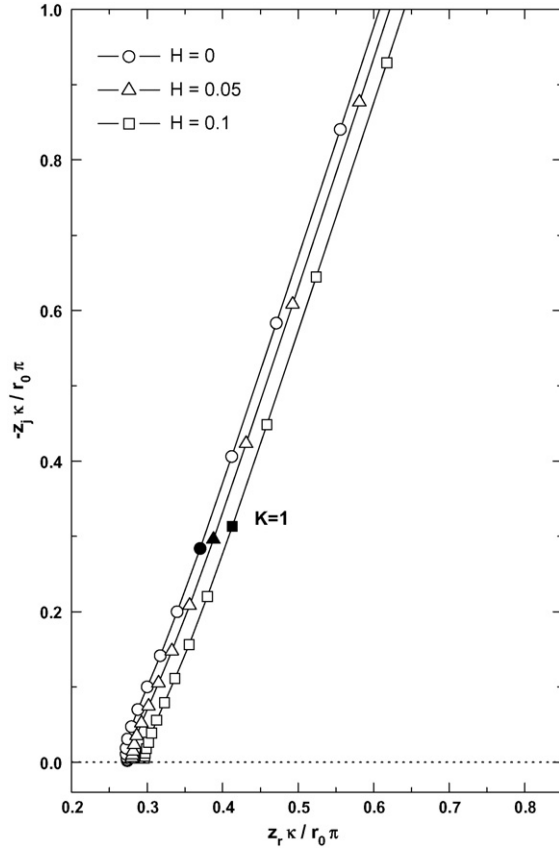

Fig. 10. Local Ohmic impedance at $r/r_0 = 0.6$ at the mouth of the recessed electrode (a) and at the electrode surface (b) with the recessed electrode depth as a parameter.

Fig. 12. Local impedances in Nyquist format at the center of a recessed electrode ($P = 0.1$) for a local CPE ($\alpha = 0.8$, $Q = 100 \times 10^{-6}\ \Omega^{-1}\ cm^{-2}\ s^{0.8}$) with the normalized probe-to-electrode distance as a parameter.

4.3. Experimental results

Fig. 14 shows the Nyquist representation of the global impedance response of a stainless steel electrode in $0.1\ M$ Na_2SO_4 electrolyte at the corrosion potential with the depth of the recessed electrode as a parameter. The electrochemical response clearly exhibits a CPE behavior. The analysis of the spectra allows $\alpha = 0.89$ and $Q = 165 \times 10^{-6}\ \Omega^{-1}\ cm^{-2}\ s^{0.89}$ to be determined. The frequency shift is ascribed to the uncompensated Ohmic drop due to the cylindrical shape of the cell as described in the previous part of the paper.

Fig. 15 shows experimental local impedance spectra for a stainless steel disk electrode at the center of the recessed electrode ($P = 0.4$) with the vertical probe position as a parameter measured at the corrosion potential. For an easiest comparison, the results are presented in dimensionless form. The parameter $H = 0.005$ represents a measurements made with the probe positioned as close as possible to the electrode surface, $H = 0.5$ represents a position at small distance above the mouth of the recessed electrode, and $H = 1$ represents a position further from the mouth of the recessed electrode. This figure is in very good agreement with the predicted shape (Fig. 12). From experimental results, it was also possible to extract the local Ohmic impedance as shown in Fig. 16 for $H = 0.5$. The local Ohmic impedance exhibits an inductive behavior at the electrode edge and a capacitive behavior at the electrode center.
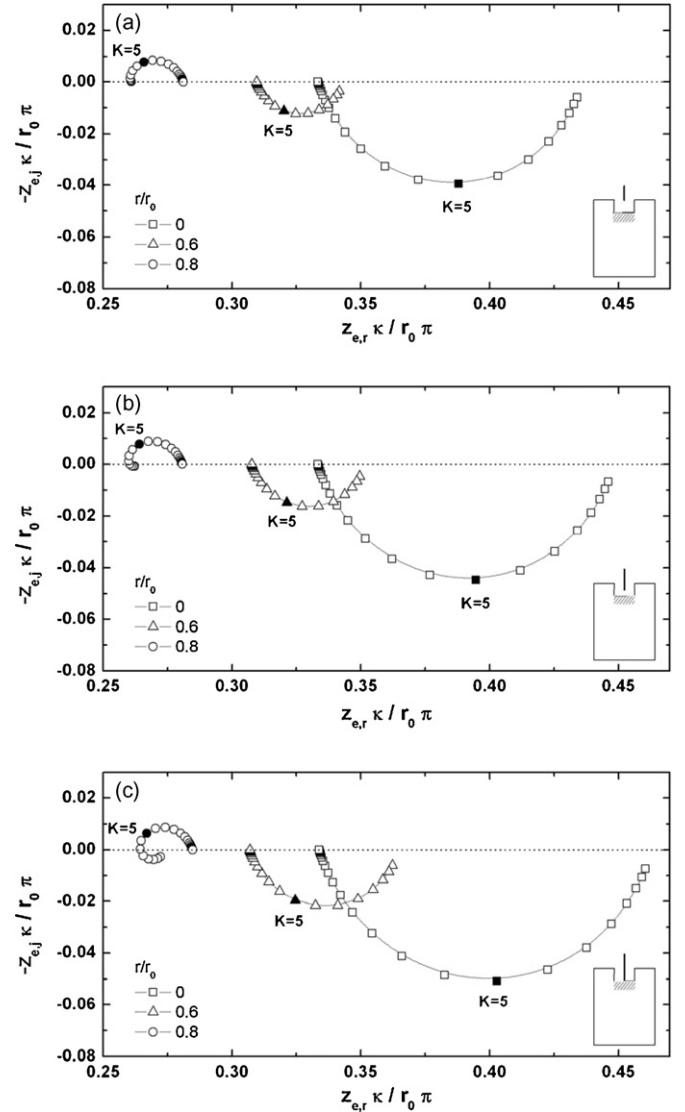

Fig. 13. Local Ohmic impedances in Nyquist format for a recessed electrode ($P = 0.1$) for a local CPE ($\alpha = 0.8$, $Q = 100 \times 10^{-6}\ \Omega^{-1}\ cm^{-2}\ s^{0.8}$) at the mouth of the recessed electrode (a); in the middle of the recessed electrode (b); and at the electrode surface (c) with the normalized radial position of the probe as a parameter.

5. Discussion

The results presented here illustrate conclusively that frequency dispersion and imaginary contributions to Ohmic impedance associated with geometry-induced current and potential distributions disappear for recessed electrodes for which the primary current distribution is uniform. A dimensionless recessed depth of $P = 2$ was found to be sufficient to eliminate frequency dispersion in the local impedance response. This result is in agreement with steady-state calculations presented by Diem et al. [22].

The calculations demonstrate also that, as discussed elsewhere [17], the height of the LEIS probe over the electrode surface represents a critical parameter for experimental investigations. Probe size and probe design are two other key parameters for LEIS measurements. Two aspects should be con-
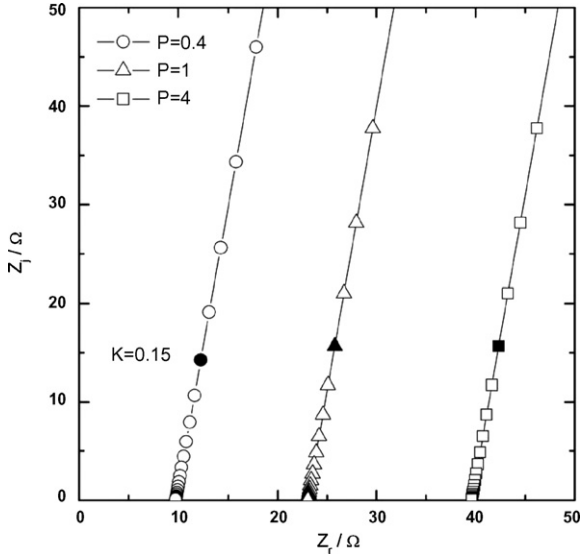
Fig. 14. Experimental Nyquist plots of the global impedance of a stainless steel electrode in Na_2SO_4 electrolyte at the corrosion potential with the depth of the recessed electrode as a parameter.

Fig. 16. Experimental local Ohmic impedances in Nyquist format for a stainless-steel disk recessed electrode ($P = 0.4$) at $H = 0.5$ with the radial probe position as a parameter. The local impedance was measured at the corrosion potential.

sidered for the probe size. The first parameter is the dimension of each of the potential sensing electrodes, which gives, in first approximation, an evaluation of the attainable resolution of the measurement. Thus, varying the probe size allows varying the resolution of the technique. However, the smaller the probe, the larger should be the input impedance of the analog device that amplify the signal for the frequency response analyzer [6]. Second, total dimension of the probe (electrode and surrounding insulators) should be also taken into account since when the probe is brought close to the disk electrode, the system can be considered as a thin layer cell leading to the confinement of species and to modifications in the diffusion behavior [20].
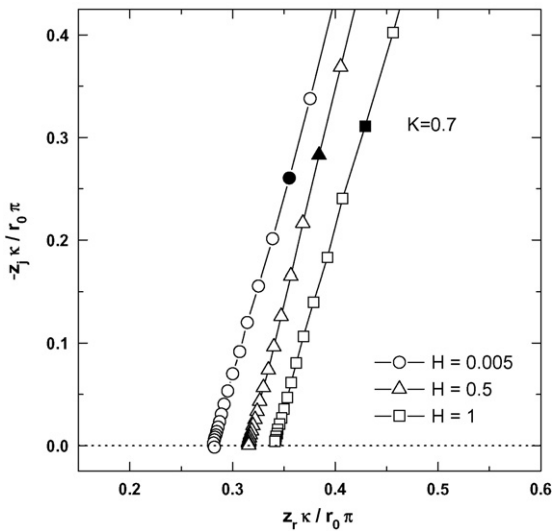
Time is a critical factor for all electrochemical impedance measurements since one assumes that the experiments are performed at steady state. However, Annergren et al. [11] have successfully used the LEIS for characterizing the electrochemical reactivity of small active area that can vary with time especially when corrosion processes are considered.

6. Conclusion

While local impedance spectroscopy provides a powerful tool for investigation of surface heterogeneities on electrode surfaces, it is influenced by geometry-induced frequency dispersion. The frequency dispersion results in inductive and/or capacitive behaviors in the high frequency range and can be eliminated by conducting measurements below a characteristic frequency $K = \omega C_0 r_0 / \kappa = 1$ or by conducting measurements on an electrode surface for which the primary current distribution is uniform. It was shown that such an ideal behavior can be obtained with the use of a recessed electrode. The calculations presented here demonstrated that the depth of the recessed electrode required to achieve a uniform primary current distribution was twice of the electrode radius. In that case, an additional Ohmic contribution due to the solution in the recessed electrode should be taken into account. The calculations also provide useful guidelines for design of LEIS measurements; especially the probe-to-electrode distance was shown to play a significant role on the magnitude of the frequency dispersion observed in the high-frequency range. The predicted behavior was in good agreement with global and local measurements performed on recessed stainless steel electrode in an inert electrolyte.

Appendix A. Nomenclature

Fig. 15. Experimental local impedances in Nyquist format for a stainless steel disk electrode at the center of the recessed electrode ($P = 0.4$) with the vertical probe position as a parameter. The local impedances were measured at the corrosion potential.
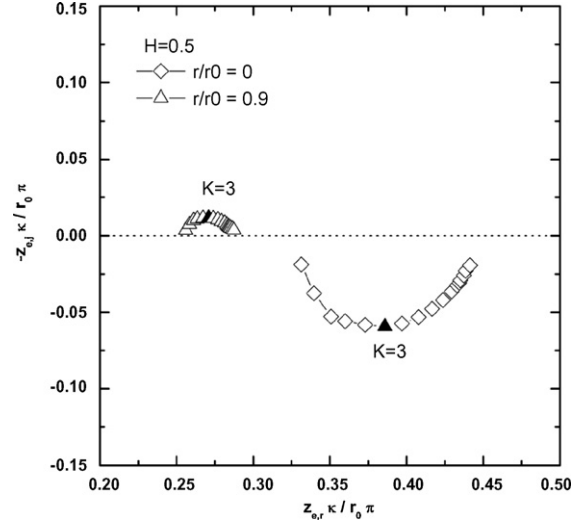
C_0	interfacial capacitance (F cm^{-2})
d	distance between the two probes (cm)

h	distance between the probe and the sample (cm)
H	dimensionless height of the LEIS probe over the electrode surface $H = h/r_0$
i_{loc}	local ac–current density (A cm^{-2})
K	dimensionless frequency $K = \omega C_0 r_0/\kappa$
p	depth of the recessed electrode (cm)
P	dimensionless depth of the recessed electrode $P = p/r_0$
Q	constant phase element (CPE) coefficient associated with the phase angle α (Ω^{-1} cm^{-2} s$^{\alpha}$)
r	radial coordinate (cm)
r_0	electrode radius (cm)
V	electrode potential (V)
ΔV_{probe}	ac–potential difference between the two probes (V)
y	axial coordinate (cm)
z	local impedance (Ω cm^2)
z_{e}	local Ohmic impedance (Ω cm^2)
$z_{\text{e},j}$	imaginary part of the local Ohmic impedance (Ω cm^2)
$z_{\text{e},h}$	local Ohmic impedance estimated at $y = h$ (Ω cm^2)
$z_{\text{e},r}$	real part of the local Ohmic impedance (Ω cm^2)
z_h	local interfacial impedance estimated at $y = h$ (Ω cm^2)
$z_{h,j}$	imaginary part of the local interfacial impedance estimated at $y = h$ (Ω cm^2)
$z_{h,r}$	real part of the local interfacial impedance estimated at $y = h$ (Ω cm^2)
z_j	imaginary part of the local impedance (Ω cm^2)
z_r	real part of the local impedance (Ω cm^2)
z_0	local interfacial impedance (Ω cm^2)
$z_{0,j}$	imaginary part of the local interfacial impedance (Ω cm^2)
$z_{0,r}$	real part of the local interfacial impedance (Ω cm^2)
Z	global impedance (Ω or Ω cm^2)
Z_j	imaginary part of the global impedance (Ω or Ω cm^2)
Z_r	real part of the global impedance (Ω or Ω cm^2)

Greek letters

Φ_{ref}	potential of the reference electrode (V)
Φ_0	potential at the inner limit of the diffusion layer (V)
α	phase angle associated with the CPE parameter Q
κ	electrolyte conductivity (Ω^{-1} cm^{-1})
π	mathematical constant
ω	frequency (s^{-1})

References

[1] A.J. Bard, L.R. Faulkner, Electrochemical Methods: Fundamentals and Applications, 2nd ed., Wiley-VCH, New York, 2001.

[2] C. Gabrielli, in: I. Rubinstein (Ed.), Physical Electrochemistry. Principles, Methods, and Applications, Marcel Dekker, New York, 1995 (Ch. 6).

[3] J. Newman, J. Electrochem. Soc. 113 (1966) 1235.

[4] J. Newman, J. Electrochem. Soc. 113 (1966) 501.

[5] W.H. Smyrl, J. Newman, J. Electrochem. Soc. 119 (1972) 208.

[6] R.S. Lillard, in: P. Marcus, F. Mansfeld (Eds.), Analytical Methods in Corrosion Science and Engineering, CRC Press, Boca Raton, 2006.

[7] H.S. Isaacs, M.W. Kendig, Corrosion (Houston, TX, United States) 36 (1980) 269.

[8] R.S. Lillard, P.J. Moran, H.S. Isaacs, J. Electrochem. Soc. 139 (1992) 1007.

[9] F. Zou, D. Thierry, H.S. Isaacs, J. Electrochem. Soc. 144 (1997) 1957.

[10] E. Bayet, F. Huet, M. Keddam, K. Ogle, H. Takenouti, J. Electrochem. Soc. 144 (1997) L87.

[11] I. Annergren, D. Thierry, F. Zou, J. Electrochem. Soc. 144 (1997) 1208.

[12] G. Baril, C. Blanc, M. Keddam, N. Pébère, J. Electrochem. Soc. 150 (2003) B488.

[13] L.V.S. Philippe, G.W. Walter, S.B. Lyon, J. Electrochem. Soc. 150 (2003) B111.

[14] V.M.-W. Huang, V. Vivier, M.E. Orazem, N. Pébère, B. Tribollet, J. Electrochem. Soc. 154 (2007) C81.

[15] V.M.-W. Huang, V. Vivier, I. Frateur, M.E. Orazem, B. Tribollet, J. Electrochem. Soc. 154 (2007) C89.

[16] V.M.-W. Huang, V. Vivier, M.E. Orazem, N. Pébère, B. Tribollet, J. Electrochem. Soc. 154 (2007) C99.

[17] I. Frateur, V.M. Huang, M.E. Orazem, B. Tribollet, V. Vivier, J. Electrochem. Soc. 154 (2007) C719.

[18] L.F. Jaffe, R. Nuccitelli, J. Cell Biol. 63 (1974) 614.

[19] C. Gabrielli, F. Huet, M. Keddam, P. Rousseau, V. Vivier, J. Phys. Chem. B 108 (2004) 11620.

[20] C. Gabrielli, M. Keddam, N. Portail, P. Rousseau, H. Takenouti, V. Vivier, J. Phys. Chem. B 110 (2006) 20478.

[21] J. Newman, J. Electrochem. Soc. 117 (1970) 198.

[22] C.B. Diem, B. Newman, M.E. Orazem, J. Electrochem. Soc. 135 (1988) 2524.